Lifetime prediction for the subsurface crack propagation using three-dimensional dynamic FEA model

Yuan Yin[1,2,3], Yun-Xia Chen[1,2], Le Liu[1,2*]

[1]School of Reliability and Systems Engineering, Beihang University, Beijing 100191, China
[2]Science and Technology on Reliability and Environmental Engineering Laboratory, Beijing 100191, China
[3]System Engineering Research Institute, China State Shipbuilding Corporation, Beijing 10094, China

Abstract

The subsurface crack propagation is one of the major interests for gear system research. The subsurface crack propagation lifetime is the number of cycles remaining for a spall to appear, which can be obtained through either stress intensity factor or accumulated plastic strain analysis. In this paper, the heavy loads are applied to the gear system. When choosing stress intensity factor, the high compressive stress suppresses Mode I stress intensities and severely reduces Mode II stress intensities in the heavily loaded lubricated contacts. Such that, the accumulated plastic strain is selected to calculate the subsurface crack propagation lifetime from the three-dimensional FEA model through ANSYS Workbench transient analysis. The three-dimensional gear FEA dynamic model with the subsurface crack is built through dividing the gears into several small elements. The calculation of the total cycles of the elements is proposed based on the time-varying accumulated plastic strain, which then will be used to calculate the subsurface crack propagation lifetime. During this process, the demonstration from a subsurface crack to a spall can be uncovered. In addition, different sizes of the elements around the subsurface crack are compared in this paper. The influences of the frictional coefficient and external torque on the crack propagation lifetime are also discussed. The results show that the lifetime of crack propagation decreases significantly when the external load T increased from 100NM to 150NM. Given from the distributions of the accumulated plastic strain, the lifetime shares no significant difference when the frictional coefficient f ranging in 0.04~0.06.

Keywords

Gear; Accumulated plastic strain; Crack growth; Finite element analysis; Life prediction

1 Introduction

Gear system is a critical subsystem in any machinery products and the gear wear is the most common failure mode [1, 2]. Wear means that the surface deterioration on the active contact profiles of machine components, e.g. gearing. Hence, the performance of gearing highly depends on the durability of tooth surface. In general, there are four basic wear modes: contact fatigue, adhesion, abrasion and corrosion, and contact fatigue is the most common mode of failure for gears under normal operating conditions.

Generally, pitting and spalling are two types of surface contact fatigue. According to [3, 4], pitting and spalling can be distinguished from two aspects: appearance and mechanism of the crack

generation. With respect to the appearance, pitting appears as shallow craters at contact surfaces with the maximum depth of a pit around 10μm, while spalling appears as deeper cavities (typically 20 - 100μm) at contact surfaces. The appearances of a pit and a spall are illustrated in Fig. 1. For the generation mechanism, Ding, et al. [3] believed that pitting results from the surface crack propagation, while spalling from the subsurface cracks that are initiated parallel to the contact surface. However, they indicated that the subsurface crack propagation will not lead to failure, and the possible reason for spalling formation is the ligament collapse spalling mechanism. The region between the crack tip and the contact surface is called ligament where the material can no longer hold its designated strength. As a result, catastrophic failure occurs with a deep cavity.

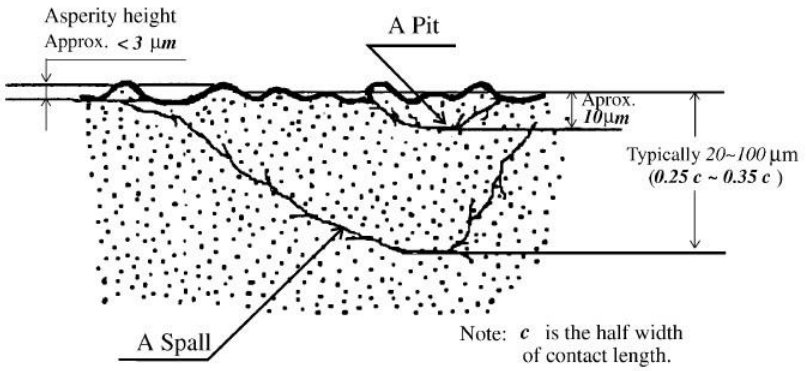

Fig. 1 The appearances of a pit and a spall[3]

Despite of a pit or a spall, the crack propagation and fatigue lifetime are always the main concern. The lifetime prediction model estimates the remaining cycles for pits or spalls to appear. The surface or subsurface crack grows with the cyclic contact loadings. Eventually, a crack becomes large enough to produce unstable growth, allowing material to break away from the surface, which results in a gradual deterioration of the surface. Failure occurs either when the surface deteriorates that the component cannot function as designed, or when the damage becomes severe enough that leads to another failure mechanism, e.g. tooth breakage [5]. Based on the stress intensity factor and Paris law, the crack propagation rate and fatigue lifetime of gearing can be given as [6]

$$\frac{da}{dN} = C\left(\Delta k\right)^m \tag{1}$$

Given from (1), the driving force behind crack growth is the cyclic change in stress intensity at the crack tip. Keer, et al. [7] proposed a line contact pitting model by assuming an initial crack with an initial angle relative to the contact surface. Mode II shear loading is used to represent the propagation driving force, and the fatigue life is given through calculating the stress intensity factor at the crack tip. Ding, et al. [8] studied the stress intensity factor ΔK_{I}, ΔK_{II} at both the leading and trailing tips of the subsurface cracks at different depths and lengths. The results show that ΔK_{I} has not exceed the threshold of crack propagation, which indicates that a subsurface crack under compressive contact loading could not be propagated in Mode I. On the contrary, ΔK_{II} is generally greater than the threshold $\Delta K_{\mathrm{II},th}$, meaning that the subsurface cracks will be propagated in Mode II. However, the highest value of ΔK_{II} is less than the critical SIF of crack failure, which demonstrates that a subsurface crack will not fail through Mode II propagation. The experimental results also show that the subsurface cracks propagating in Mode II are approximately parallel to the contact surface. Komvopoulos, et al. [9] selected linear elastic fracture mechanics and finite element

simulations to analyze subsurface cracking in a homogeneous half-space due to a moving asperity. The focus is on the direction and the rate of crack propagation due to indentation and sliding contact. The crack propagation directions in shear and tensile mode can be predicted based on the maximum range of the shear and tensile stress intensity factor. The results show that the maximum values of shear stress intensity factor ΔK_τ at both crack tips occurs at θ = 0°, whereas tensile stress intensity factor ΔK_σ at the left and right tips occur at θ = 70.5° and -70.5° respectively, where θ is the polar coordinate at the crack tips. The results demonstrate the horizontal subsurface crack would exhibit in-plane growth when the shear mechanism was dominant, which is in accordance with Ding, et al. [3]. In addition, if the tensile mechanism is responsible for the commencement of crack growth, propagation from the left tip would tend to occur toward the surface and from the right tip downward into the half-space.

Besides the studies on single stress intensity factor, efforts have been devoted to the mixed mode stress intensity factors. In Aslantas, et al. [10], $\Delta K_{eff}^4 = \Delta K_I^4 + 8\Delta K_{II}^4$ is defined to evaluate mixed mode stress intensity factors K_{I}, K_{II} at the subsurface crack tip, and then propagated to crack extension with Paris-type equation. The results show that the values of K_{I} are always negative under all load positions. Thus, the negative K_{I} is assumed to be zero since that it has no effect on crack growth. So the subsurface crack growth is dominated by K_{II} and $\Delta K_{eff}^4 = 8\Delta K_{II}^4$. However, the maximum tangential stress criterion is used to determine the crack growth direction, and the results indicates that subsurface crack could grow toward the surface and form a pit (spall) eventually.

The above mentioned studies are proposed under two-dimensional finite element simulation. Recently, special attentions are given to the three-dimensional finite element simulations [11, 12]. Ural, et al. [13] applied three-dimensional FEA model to predict crack shape for a spiral bevel pinion gear based on linear elastic fracture mechanics, combining with finite element method and incorporating plasticity-induced fatigue crack closure and moving loads, where K_{I} is that of interest. Lin, et al. [14] established a three-dimensional boundary element model of cylindrical gear with crack in tooth root, and calculated the stress intensity factors K_{I}, K_{II}, K_{III} using the opening displacement, sliding displacement and tearing displacement of the crack tip.

Despite of that utilizing the stress intensity factor and Paris law to determine the crack growth rate and fatigue life, extensive works have applied plastic deformation to study the crack propagation and fatigue life. A Hertzian pressure profile is generally used to determine the stress intensity factor. However, the pressure distribution in lubricated contacts is significantly different from that of the Hertzian. In addition, during heavily loaded lubricated contacts, high compressive stress in the contact zone virtually suppress Mode I stress intensities, and severely reduce Mode II stress intensities through the action of high friction between the crack faces [15]. Hence, the stress intensity factors based on the linear elastic fracture mechanics is not applicable for the situations of heavy loads that may result in plastic deformation. Bower, et al. [16] proposed that the fatigue spall initiation and propagation are due to the accumulated plastic strain process rather than stress intensity at the crack tip. Since that the accumulated plastic deformation in the contact layer is formed with repeated loading, micro-cracks are initiated in the layer. With the continuous plastic strains, the micro-cracks could move to the surface and eventually lead to a relatively large spall. Then the spall may continue to propagate, resulting in a large scale rolling contact fatigue spall. Johnson [17] reviewed the research of Cambridge on the mechanics of plastic deformation under surface and subsurface layers in rolling and sliding contact. Four possible regimes of behavior are identified to ascend load: perfectly elastic, elastic shakedown, plastic shakedown or cyclic plasticity,

incremental collapse or ratcheting. A simple non-linear kinematical hardening model of material behavior is also given, which achieves excellent prediction performances of ratcheting rate in line contact. Cheng, et al. [18] proposed a model to predict crack initiation life (the cycle numbers the contact undergoes until crack initiates) under contact fatigue based on dislocation pileup theory, where the influence of residual stress, hardness, irreversibility of plastic deformation and many other parameters on the crack initiation life are discussed. Xu, et al. [15] proposed an analytical model to investigate the effects of dent on spall initiation and propagation in lubricated contacts based on the damage mechanics concept, where the fatigue spall initiation and propagation are results from the accumulated plastic strain rather than the stress intensity at the tip of the crack. A dent profile from finite element analysis is used for a spherical debris denting the contact surface. Spall size and growth rate versus cycle number are presented. The results indicate that spall always initiates at the dent edge. Kang, et al. [19] investigated the effects of contaminants in heavily loaded rolling and sliding contacts by developing a dynamic time dependent finite element model in order to determine the elastic-plastic deformation and contact force generated between the mating surfaces and a spherical debris when debris passing though the contact region. The effects of various parameters are obtained, such as debris size, material properties, frictional coefficients, applied loads and surface speeds on the elastic-plastic deformation and contact force of the system. Arakere, et al. [20] investigated the rolling contact fatigue initiation and spall propagation characteristics of different bearing materials. Elastic and elastic-plastic subsurface stress fields are computed using finite element models that incorporates the full three-dimensional ball-raceway geometry. The results show that there are extensive yielding at the spall edges due to ball rolling contact, and the impact loads result in extensive plastic deformation of the spall trailing edge, leading to degradation and release of material resulting in spall propagation.

In summary, the main research on the subsurface or surface crack in gears generally selects the two-dimensional finite element model, or applies the static gear model, where the surface contact loads are artificially defined and applied along with the contact surface to calculate the stress or strain for gears. In this paper, we assume that a subsurface defect exists in one tooth of a pair of heavy loaded spur gears to study the crack propagation and lifetime of spur gears. A dynamic analysis of gear engagement is performed with the three-dimensional finite element model using ANSYS Workbench transient analysis. Therefore, the time-varying sliding-rolling contact loads due to the gear engagement can be obtained to compute the stress or strain for each time increment. The defective tooth is divided into many small elements in the finite element model. In this study, the accumulated plastic deformation of each element near the subsurface crack is selected to decide the crack propagation and fatigue life. In addition, the influences of different sizes of these adjacent elements are compared in order to decide the optimal element size. Different loads are applied to the wheel gear to study the relationship between loads and crack propagation time. Meanwhile, the effects of the various frictional coefficients on contact surfaces are also studied.

This paper is organized as follows: Section 2 introduces the gear subsurface defect model in ANSYS Workbench transient analysis. Section 3 describes the calculation procedure of the subsurface crack propagation based on the accumulated plastic strain of each element near the crack. In Section 4, the effects of element size, frictional coefficient and external load on the crack propagation time are discussed. In addition, the normal and shear stresses of the two crack tips that are close to the addendum and tooth root are calculated through the linear elastic FEA model. Section 5 concludes this paper.

2 Gear subsurface defect model

The finite element analysis (FEA) model is generally used to analyze crack propagation. In this study, ANSYS Workbench is selected to establish the FEA model, and obtained the stress and strain results that of interest. The three-dimensional spur gear model is illustrated in Fig. 2. The coupled rigid and flexible mode are proposed to simulate the mesh motion between the defective gear and the normal gear. As shown in Fig. 2, the pinion gear and wheel gear under study have five flexible teeth, while the rest are rigid components that will not be deformed in the calculation. The subsurface defect is located at one of the flexible teeth of pinion gear, whose stress and strain results are of the main concern.

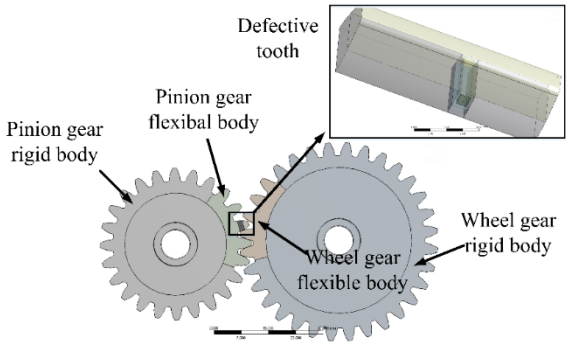

Fig. 2 The gear FEA model

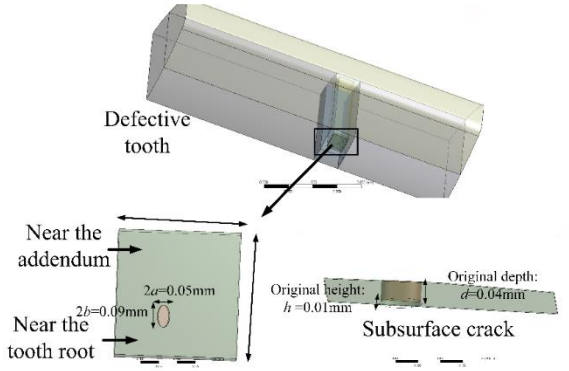

Fig. 3 The size and location of the defect in the tooth

In order to locate the subsurface crack, a block with 0.5mm × 0.5mm × 0.05mm is removed from the face of the defective tooth near the pitch line, and one crack in the shape of the coin is located on this block, see Fig. 3. The crack is set on the subsurface, and the original sizes are $2a$=0.05mm, $2b$=0.09mm, h=0.01mm and d=0.04mm. The original sizes and depths of the subsurface crack are defined after [10, 13]. To avoid the geometrical incompatibilities of the deflected tooth, the defective tooth is divided into eight regular parts. After that, the block (where the subsurface crack locates) and the rest part of this tooth are grouped into one multibody part using "form new part" tool in ANSYS Workbench, which enables the use of shared topology among the bodies to obtain high quality mesh.

The FEA model of the spur gears is shown in Fig. 4. The element type of the chipped rectangular solid is solid 186, and the most suitable size of these elements in FEA model will be discussed in Section 4.1. The dense mesh near the defective part ensures the accurate prediction results for the crack propagation.

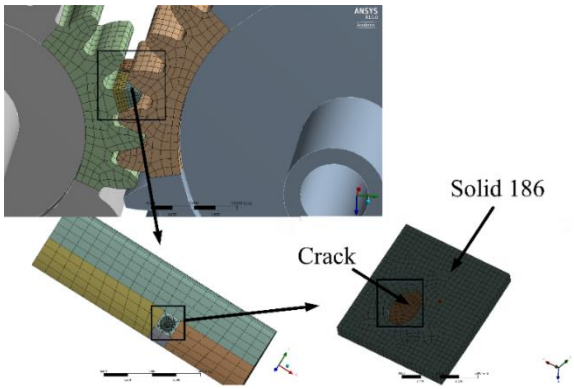

Fig. 4 The FEA model of the spur gears

The basic information of the pair of spur gears is given in Table 1.

Table 1 The basic data of the pair of spur gears

	pinion	**wheel**
Gear material	40CrNiMoA	
Pitch diameter (mm)	38.1	50.8
Number of teeth	24	32
Tooth width (mm)	10	10
module	1.6	1.6
Base diameter (mm)	35.8	47.7
Pressure angle on pitch circle	20°	20°
Fixed blend radius (mm)	0.4	0.4

The pinion gear has a speed of 5000RPM and rotates clockwise by 30 degrees to ensure that the defective tooth can experience the whole meshing period. The original position of the pinion gear is shown in Fig. 2, while its teeth contact path is illustrated in Fig. 5. The wheel gear is applied external torque ranged from 100NM to 150NM and rotates anticlockwise. Therefore, the transient sliding-rolling contact loads between the surfaces of the gears will be produced to obtain the transient accumulated plastic strain and stress directly from the ANSYS Workbench. Then the propagation time of the subsurface crack can be calculated using dynamic analysis though the methodology given in Section 3.

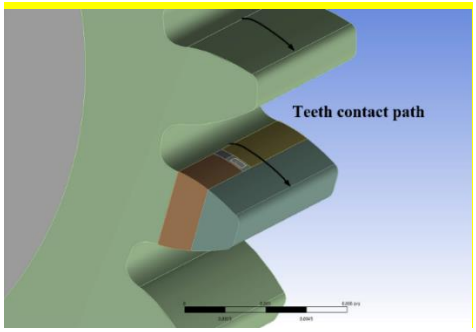

Fig. 5 The path of teeth contact for pinion gear

Noted that the friction coefficient *f* between contact surfaces cannot be ignored. In the general case of gear tooth contact at well-lubricated condition, the surface traction is low with a friction coefficient *f* about [0.04, 0.06] [4]. Thus, *f* is set as 0.04 and 0.06 to study the effects of different friction coefficients on the contact surfaces.

3 Calculation of the crack propagation time

3.1 Damage variable for crack propagation

The defective tooth is divided into small elements, especially near the area where the subsurface defect happens. Each element is a representative volume element from the view point of the continuum mechanics, and it is small enough that every physical quantity can be treated as the evenly distributed constants [15]. For each element near the defect, a damage variable D is defined as

$$D = \frac{V_D}{V} \tag{2}$$

where, V_D is damage volume, V is the total volume of the element. D = 0 means the element is undamaged, and D = 1 indicates fully damaged.

Based on the damage law by Lemaitre [21], the damage accumulation process of the element is

$$\frac{dD}{dN} = \frac{Y}{S_m}\frac{dE_p}{dN} \cdot H\left(E_p - E_{pD}\right) \tag{3}$$

where, S_m is the material constant, E_p is the accumulated plastic strain that is the sum of plasticity of each element around the fault and is also a function of cycle number N, E_{pD} is the critical plastic strain below which no damage will occur. According to Xu, et al. [15], S_m and E_{pD} can be determined accurately by experimental tests for different materials, where E_{pD} = 0.1 is recommended and S_m = 4×10^6 is selected for our study. H is a step function as

$$\begin{aligned} H\left(E_p - E_{pD}\right) &= 0, E_p \le E_{pD} \\ H\left(E_p - E_{pD}\right) &= 1, E_p > E_{pD} \end{aligned} \tag{4}$$

When the accumulated plastic strain exceeds the critical strain, the damage is accumulated with the defect growing. Thus, Eq.(3) can be applied. Y is the strain energy density release rate defined as

$$Y = \frac{\sigma_{Mises}^2 C_{tr}}{2E\left(1-D\right)} \tag{5}$$

where, σ_{Mises} is the Von Mises stress of each element, E is elasticity modulus, D is the accumulated damage of each element, and C_{tr} is the triaxiality coefficient.

$$C_{tr} = \frac{2}{3}\left(1+\nu\right) + 3\left(1-2\nu\right)\left(\frac{\sigma_h}{\sigma_{Mises}}\right)^2 \tag{6}$$

where, ν is the Poisson ratio, $\sigma_h = (\sigma_x + \sigma_y + \sigma_z)/3$, σ_x, σ_y, σ_z is the normal stresses for each element. All σ_{Mises}, σ_x, σ_y, σ_z are varied with time step t in one cycle due to the transient analysis.

In the numerical procedure, there is a damage variable $D_i(N+1)$ associated with element i in the $(N+1)^{th}$ cycle, which can be obtained from the element's damage in the N^{th} cycle $D_i(N)$:

$$D_i\left(N+1\right) = D_i\left(N\right) + \int_1^{end} \frac{Y}{S_m}\left(\Delta\varepsilon_p\left(t\right)\right)_i H\left[\left(E_p\left(N\right)\right)_i - E_{pD}\right]dt \tag{7}$$

where, $(\Delta\varepsilon_p(t))_i$ is the increment of the accumulated plastic strain in each time step of one cycle for element i. Herein, the accumulated plastic strain for element i, i.e. $(E_p(N))_i$, is directly obtained in

each time step of one cycle from FEA though ANSYS Workbench.

When the damage variable $D_i(N+1)$ reaches 1, the corresponding element is damaged. Then, the lifetime (or the total cycle number) for each element can be calculated through Eq.(7). The detailed calculation procedure is proposed in Fig. 6.

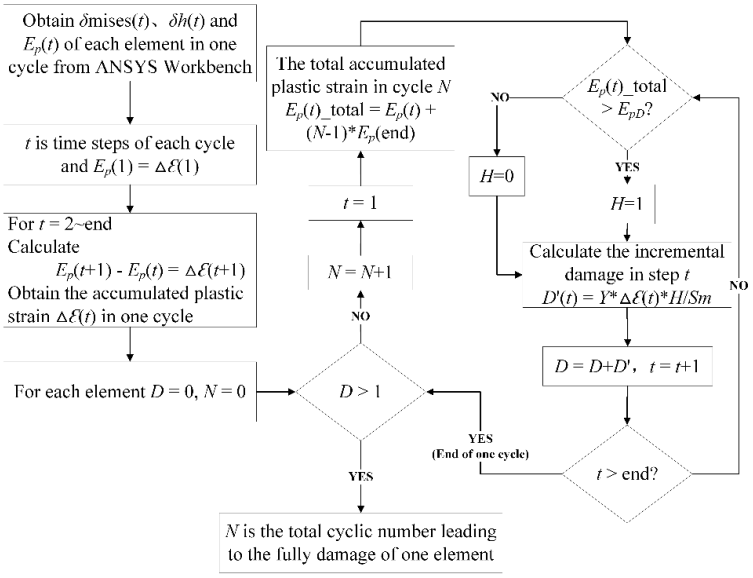

Fig. 6 The calculation procedure of total cycle number of one element

To obtain the plastic deformation, the bilinear kinematic hardening strain-stress relationship is employed in the procedure of simulation computation. The initial slope of the curve is the elastic modulus of the material E. When it arrives the specified yield stress σ_0, plastic strain will develop, while the back stress will evolve that stress versus strain will remain a linear relationship, see Fig. 7. The corresponding slope is defined by the specified tangent modulus E_T [22]. In this paper, σ_0 = 1050MPa and E_T = 2090MPa.

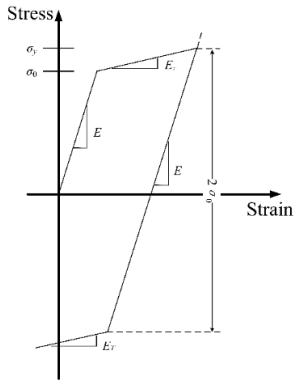

Fig. 7 Stress vs. total strain for bilinear kinematic hardening

3.2 The crack propagation time

Due to the presence of crack, the adjacent elements are small in size but large in number, which is illustrated in Fig. 4. During one cycle, the defective tooth goes though the double teeth-meshing area, the single teeth-meshing area and the double teeth-meshing area in sequence, and the plastic strain of adjacent elements occurs. Through ANSYS Workbench Transient Analysis, we can obtain the accumulated plastic strain of these elements in one cycle, which then will be used to calculate the total cycle number for elements following the procedure in Fig. 6.The crack propagation time is

based on the cycle numbers of these elements.

Fig. 8 I, II, III (b) shows the plastic strains of these elements near the crack are accumulated during one cycle. The elemental mean results of each deformed element, including accumulated plastic strain, equivalent stress and mean stress, are used to compute the total cycle number through the procedure in Fig. 6. When all those plastically deformed elements near the crack are damaged, it can be assumed that the subsurface crack propagates to the region of these elements. After that, the crack profile should be modified accordingly. The entire process will iterate until the crack propagates to the contact surface, eventually form one deep cavity, see Fig. 8. Details about the whole iterative process is given in Fig. 9.

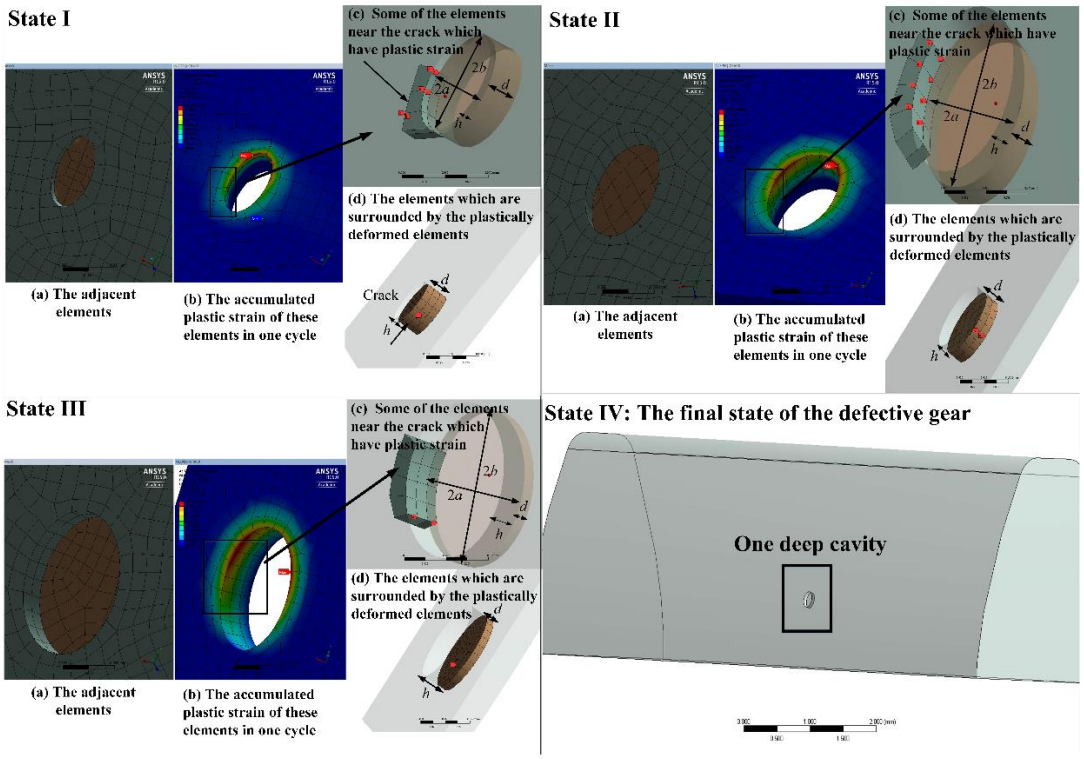

Fig. 8 The demonstration of the calculation process

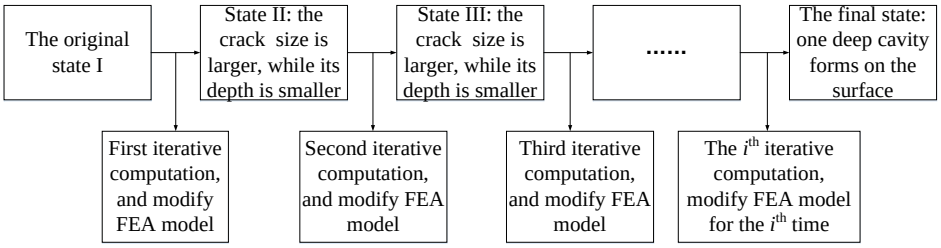

Fig. 9 The iterative process flow chart

Noted that different element size near the subsurface crack may lead to different iteration times, crack size and the final crack propagation time. Such that, special attention must be paid to the element size near the subsurface crack. The demonstration of the whole process is illustrated in Fig. 8, in which the subsurface crack is in light white color. As shown, larger $2a$, $2b$ and h results in smaller d after each iteration, which means that the crack becomes larger and locates closer to the contact surface. In fact, during the subsurface crack propagation, the region surrounded by plastically deformed elements would not peel off the gear until the crack propagates to the surface,

but has little effect on the analysis of crack propagation, see Fig. 8 I, II, III (d). Therefore, in order to achieve a regular and simplified subsurface crack model that can gain the convergent results with high efficiency, we modify the crack profile each time by ignoring the elements in this region.

4 Results and Discussion

4.1 Discussion on the different element sizes

In order to use the plastic strain of the elements near the crack to investigate the subsurface crack propagation, the targeted elements need to be small enough to guarantee reasonable strain or stress results. However, it is quite difficult to explicitly define the size of these elements since different element size near the crack may lead to different iteration times, crack and final crack propagation time. Therefore, the element size need to be selected carefully. The element sizes are selected as 0.010mm, 0.015mm, 0.020mm, 0.025mm, 0.030mm, 0.035mm and 0.040mm for comparison.

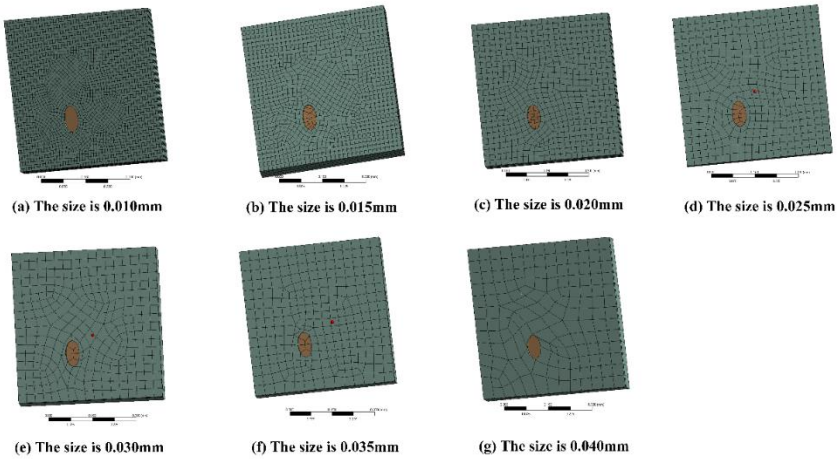

Fig. 10 The FEA models based on different element sizes

Table 2 The average of skewness with different size of element

The element size(mm)	**0.01**	**0.015**	**0.020**	**0.025**	**0.030**	**0.035**	**0.040**
The average of skewness	0.119	0.160	0.165	0.176	0.202	0.209	0.212

To select the optimal size of element, a quality measure for a mesh named skewness is applied with the range from 0~1, where zero indicates a best element, and one indicates a worst element, see Table 2. It can be seen that the elements near the crack are not uniform and most of them are highly skewed with the sizes of 0.030mm, 0.035mm and 0.040mm, also see Fig. 10 (e), (f) and (g), which may lead to terrible simulation results. On the contrary, better elements around the crack are obtained when the size is 0.010mm in Fig. 10 (a). However, the total element number is more than 50000, which is rather time-consuming to compute. Thus, the sizes of 0.015mm, 0.020mm, and 0.025mm are chosen for comparison. The crack propagation time and relevant results are listed in Table 3, where the maximum iteration is equal to the times of model modification to form a cavity on the surface.

From Table 3, the maximum possible size of the final crater for 0.025mm is larger than that of 0.015mm, while the total cycle number is lower, which is not true in reality. As a result, the sizes of 0.015mm and 0.020mm are more appropriate. For more precise results, 0.015mm is selected as the

optimal element size.

Table 3 The final crack propagation time

Element size (mm)	Maximum iteration	The calculated cycle number of each iteration			Final crack propagation time/Total cycle number	The crater maximum possible size (2a×2b/mm)
		1	2	3		
0.015	3	6.6×10^{7}	4.8×10^{7}	7.0×10^{7}	1.84×10^{8}	0.07×0.09
0.020	3	1.43×10^{8}	4.4×10^{7}	5.2×10^{7}	2.39×10^{8}	0.085×0.105
0.025	2	5.6×10^{7}	4.9×10^{7}		1.05×10^{8}	0.075×0.095

With the element size of 0.015mm under the condition of T = 100N and f = 0.06, the calculated cycle numbers to each state are listed in Table 4. The tooth contact pressure maps relative to the fault location for state I-III is shown in Fig. 11 at $t = 0.19\times10^{-3}$s and 0.27×10^{-3}s respectively. Details are given in the supplementary material. Herein, state I is the initial state of the gears as illustrated in Fig. 3. The crack size and depth for each state are also given with their appearances in Fig. 12. After the third iterative in state III, the model is modified for the third time and a cavity is formed on the contact surface, which is state IV.

Table 4 The calculation results in each state

	The cycle numbers to the state	The size of the crack		The depth of the crack	
		2a	***2b***	***h***	***d***
State I		0.05	0.09	0.01	0.04
State II	6.6×10^{7}	0.08	0.12	0.024	0.026
State III	1.14×10^{8}	0.11	0.15	0.038	0.012
State IV	1.84×10^{8}	0.14	0.18	0.05	0

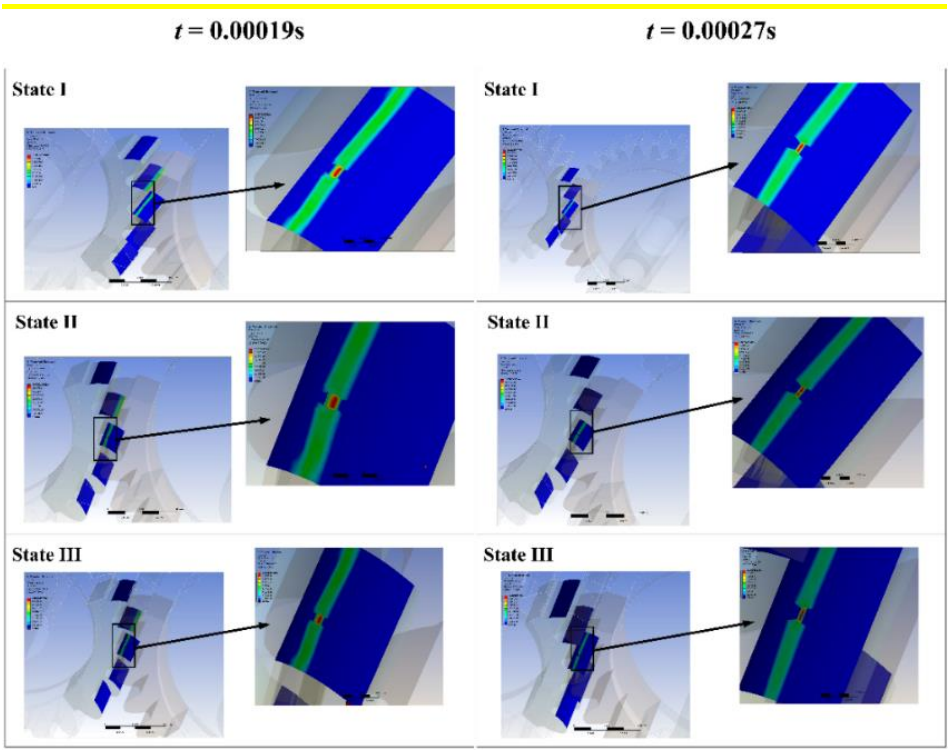

Fig. 11 The tooth contact pressure maps relative to the fault location

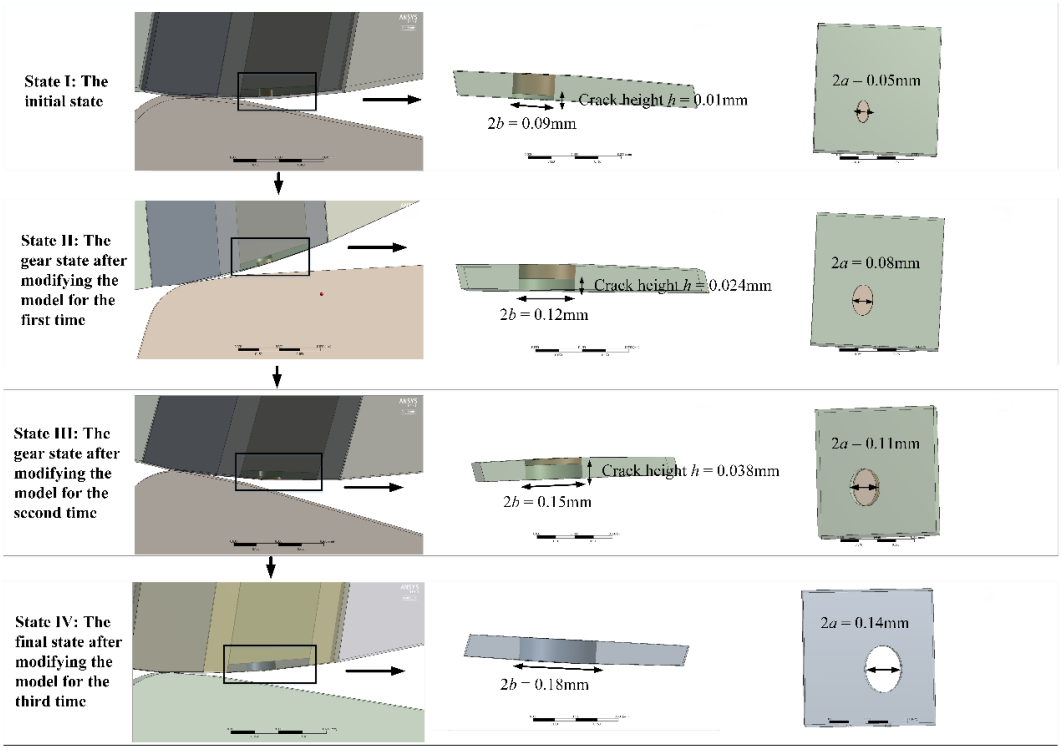

Fig. 12 The crack appearance in each state

4.2 Results at different frictional coefficients

Under the conditions of $f = 0.04$ and 0.06, the external torque $T = 100$NM and the pinion speed of 5000RPM, the time-varying global maximum values of accumulated plastic strain distributed over the defective tooth in one mesh cycle for the first three state (state I, II, III in Fig. 12) are illustrated in Fig. 13. Each curve presents the strain output calculated by ANSYS Workbench of different states in different conditions during one mesh cycle of the defective tooth. It is shown that the plastic strain starts to accumulate when the defective tooth comes to engage under both conditions in period B, and the maximum accumulated plastic strains increase almost at the same time periods, which are about 0.16×10^{-3}s ~ 0.19×10^{-3}s and 0.27×10^{-3}s ~ 0.37×10^{-3}s in period B and period D. However, the final maximum value of accumulated plastic strain in the case of $f = 0.06$ is slightly larger than that in the case of $f = 0.04$ for each iteration, which may due to the higher friction caused by higher frictional coefficient.

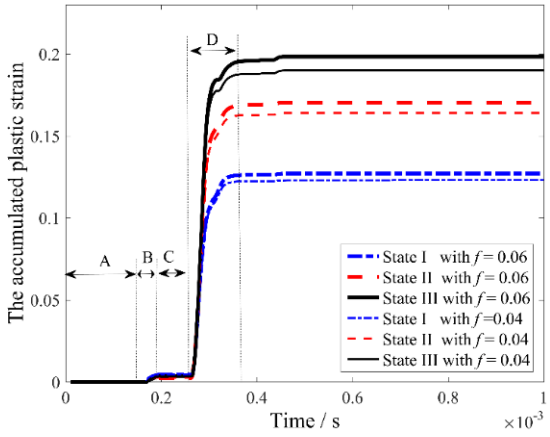

Fig. 13 The accumulated plastic strain vs time in the case of different f

At $t = 0.19\times10^{-3}$, the global maximum accumulated plastic strain remains unchanged after the first rise in period B, and reaches their maximum values at $t = 0.5\times10^{-3}$s. The distributions of the accumulated plastic strain at the two specific time are shown in Fig. 14. The results demonstrate that the maximum accumulated plastic strain takes place around the edge of the subsurface crack. When the defective tooth is in the state III, the elements on the contact surface begin to damage, meaning that the crack has propagated to the surface. When $t = 0.19\times10^{-3}$s, the contact load moves from tooth root to the edge of the crack. Thus, the accumulated plastic strain reaches its maximum value over the period B, which are about the double teeth meshing period for the defective tooth.

With the contact loads moving, the plastic strain over this tooth continue to accumulate, but the accumulated value is still less than that at $t = 0.19\times10^{-3}$. Therefore, the accumulated plastic strains experience no apparent growth during 0.19×10^{-3}s ~ 0.27×10^{-3}s in period C. Then, the defective tooth starts single teeth meshing in period D, and the accumulated plastic strain increase sharply around the crack end near the addendum. Eventually, the accumulated plastic strain in this area reaches globally maximum.

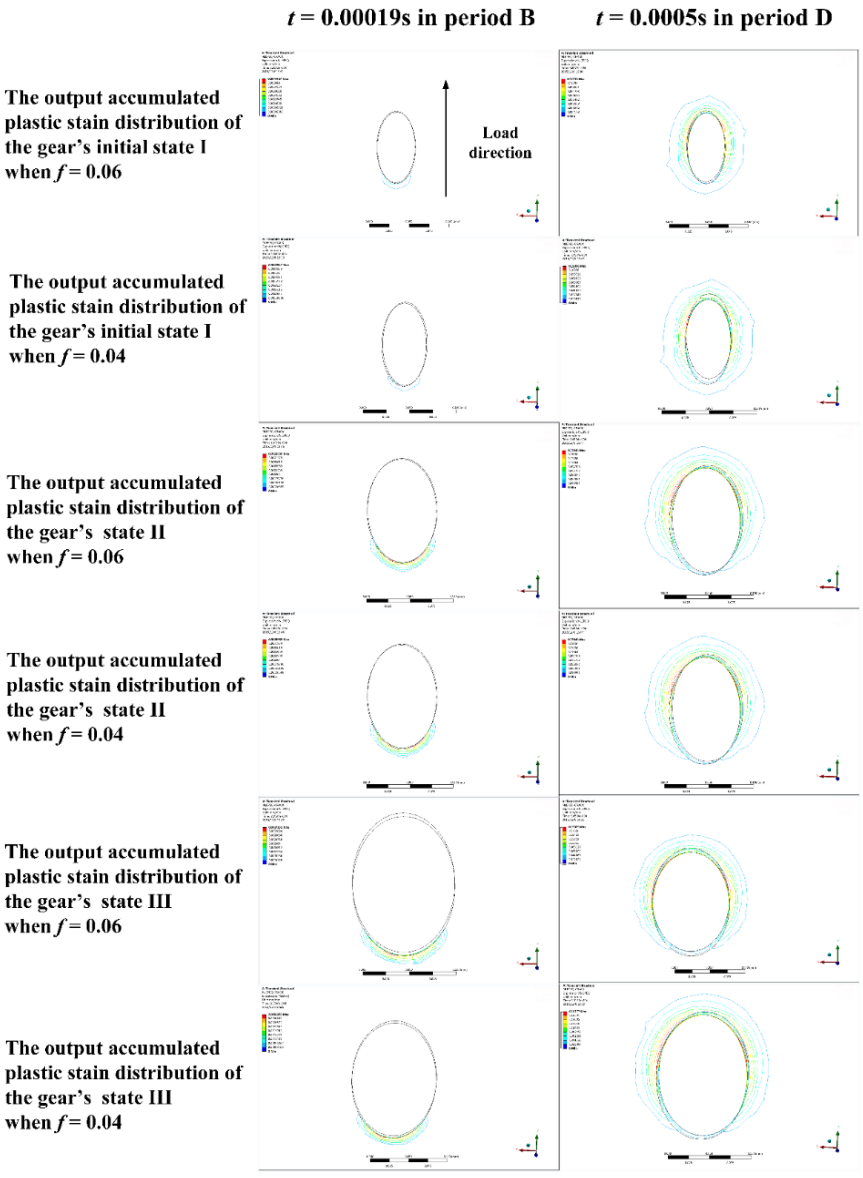

Fig. 14 The accumulated plastic strain distributions under different f

Besides the global maximum value of the accumulated plastic strain, the value for any target elements in one cycle of each gear state are also obtained from the FEA model. For each state, there are more than 30 elements around the crack that have plastic deformation and the total cycle number of each element can be calculated. The crack propagation time based on each element total cycle number in the case of f = 0.04 and 0.06 is illustrated in Fig. 15. In each state, the total cycle numbers for the first six and the last four completely damaged elements are showed. As shown, the crack propagation time in the case of f = 0.04 is about 1.9×10^8 cycles, which is a little bit larger than 1.84×10^8 cycles when f = 0.06. Hence, it can be concluded that the total cycle numbers in the two cases shares no significant difference, which means the friction coefficient has little effect on the crack propagation time within the reasonable range (about 0.04~0.06).

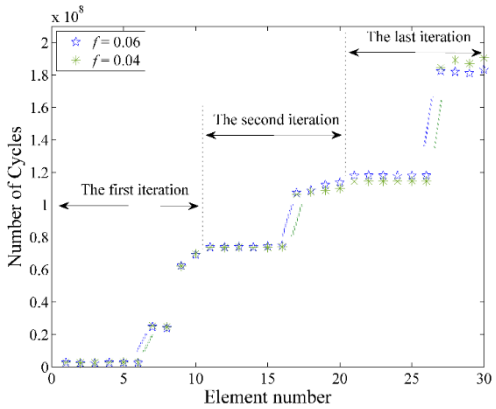

Fig. 15 The crack propagation time in the case of different f

4.3 Results at different loads

Under the conditions of T = 150NM and 100NM, the frictional coefficient f = 0.06 and the pinion speed of 5000RPM, the time-varying global maximum values of accumulated plastic strain over the defective tooth in one mesh cycle for the first three state (state I, II, III in Fig. 12) are illustrated in Fig. 16. It can be seen that the plastic strain over the defective tooth is accumulated earlier in period B for T = 150NM, and its value is larger than that from T = 100NM after the defective tooth engages. Under T = 150NM, the maximum accumulated plastic strains increase significantly in period B and D. During this two periods, the contact load moves from tooth root to the edge of the crack and the defective tooth begins single teeth meshing. Such situation is the same for T = 100NM.

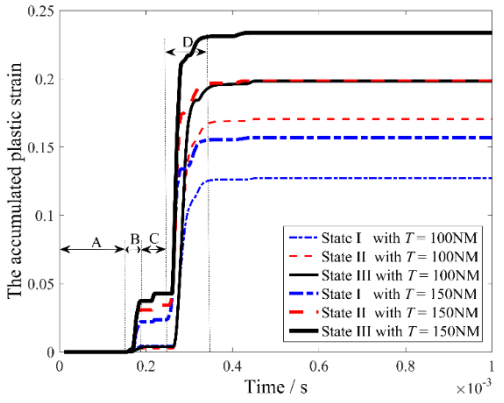

Fig. 16 The maximum accumulated plastic strain vs. time in the case of different T

In terms of the accumulated plastic strain, it increases slightly for T = 150NM when t = 2.2×10^{-4}s ~ 2.4×10^{-4}s for period C. The distributions of accumulated plastic strain when t = 0.19×10^{-3}s, 0.24×10^{-4}s and 0.5×10^{-3}s are shown in Fig. 17. It could be derived that the elements around the crack tips are not damaged earlier than other elements around the crack.

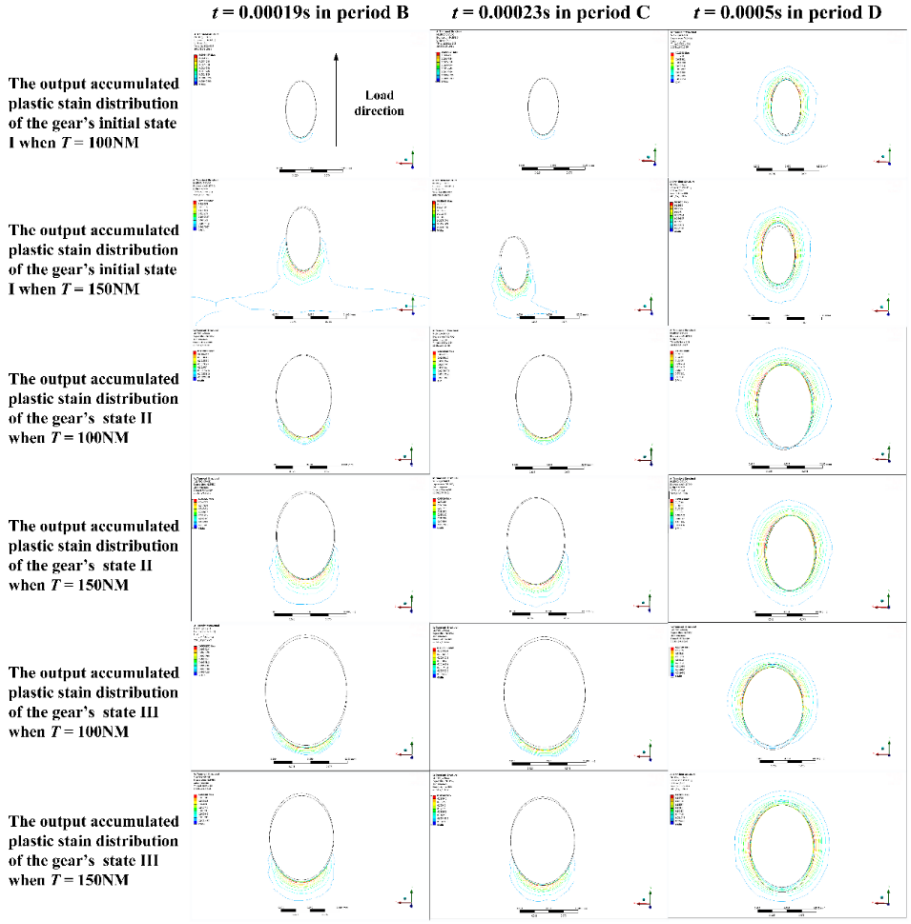

Fig. 17 The accumulated plastic strain distribution under different T

The crack propagation times based on the total cycle number are illustrated in Fig. 18 for T = 100NM and 150NM. It is clear that the crack propagation time when T = 150NM is about 6.6×10^{7}, which is much less than 1.84×10^{8} under T = 100NM.

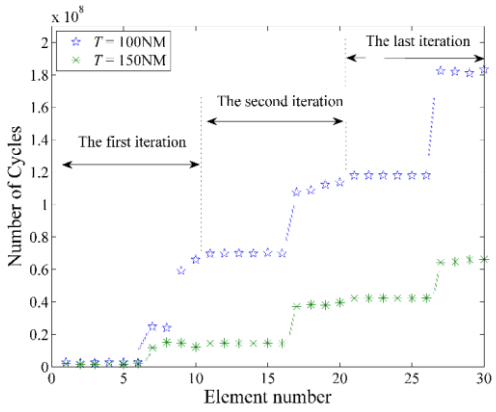

Fig. 18 The crack propagation time in the cases of different T

4.4 Discussion on the stress results with linear elastic FEA

For comparison, the normal and shear stresses of the two crack tips (close to the addendum and tooth root) are proposed with the pinion speed 5000turns/min. The rectangular coordinate systems at the two crack tips are shown in Fig. 19. The calculated stress results are given in Fig. 20 and Fig. 21.

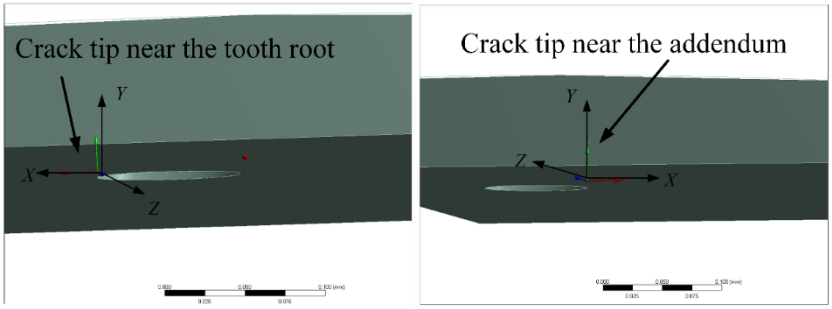

Fig. 19 The rectangular coordinate systems at the crack tips

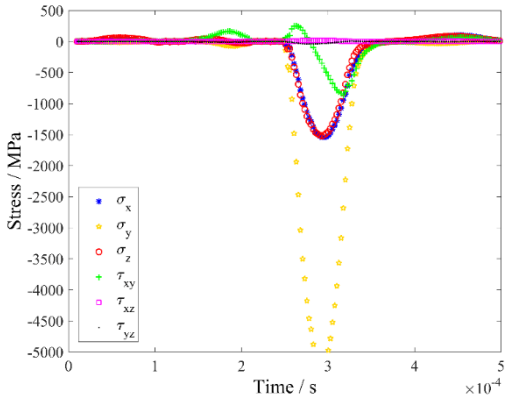

Fig. 20 The normal & shear stresses of the crack tip near the addendum

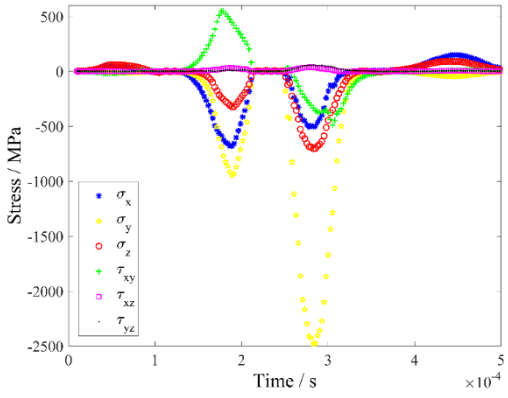

Fig. 21 The normal & shear stresses of the crack tip near the tooth root

Given from Fig. 20 and Fig. 21, it can be seen that the shear stress τ_{yz} and τ_{xz} are negligible compared with τ_{xy}. Meanwhile, the normal stresses are almost all negative and their absolute values are very large over the whole meshing period, which is considered as no effect on the subsurface crack growth based on the stress intensity factors theory. If it is simplified to a XY plane problem, there will be only K_{II}, which means the subsurface cracks propagation is dominated mainly by Mode II. According to Y Ding [3, 4, 8] and K. Komvopoulos [9], the subsurface propagates parallel to the

surface if it is dominated by Mode II. The value of K_{II} calculated by τ_{xy} is always small at the crack tips. Therefore, the spalling could not be formed only in Mode II. It has been proved that under heavily loaded contacts, Mode I and II stress intensities will be suppressed and significantly reduced by the high compressive stress in the contact zone, respectively.

5 Conclusion

In this paper, we proposed a method to calculate the lifetime of the subsurface crack propagation time. The accumulated plastic strain is applied instead of stress intensity factors for the heavily loaded lubricated contacts. By using ANSYS Workbench, the FEA model of one pair of gears is built with a subsurface crack in a tooth of the pinion. The gear system is divided into small elements especially for the defective tooth. The computation of the subsurface crack propagation time is based on the time-varying accumulated plastic strain, equivalent stress and mean stress of these elements around the subsurface crack. The proposed method has been demonstrated to be efficient and accurate by just applying external torque and speed to the gear system to get the time varying results through the transient analysis without using the contact loads.

The influences of the frictional coefficient and external torque on the crack propagation lifetime are also discussed. Under different frictional coefficients with external load T =100NM, the maximum accumulated plastic strain majorly increases over the same two time periods: 0.16×10^{-3}s ~ 0.19×10^{-3}s and 0.27×10^{-3}s ~ 0.37×10^{-3}s, which are period B and period D respectively. Under T =150NM, the maximum accumulated plastic strain also increases in period C when $t = 2.2\times10^{-4}$s ~ 2.4×10^{-4}s. The final maximum value of accumulated plastic strain for $f = 0.06$ is slightly larger than that for $f = 0.04$, while the crack propagation time for $f = 0.04$ is longer than that for $f = 0.06$. The accumulated plastic strain distribution in various time is also investigated. The results show that the lifetime of the crack propagation shares no significant difference when the friction coefficient is within a reasonable range (about 0.04~0.06).

The crack propagation time under T = 150NM is much shorter than that under T = 100NM. Combined the results from the accumulated plastic strain distribution in different frictional coefficients or loads, it could be derived that the crack tips are generally not damaged earlier than other edges of the crack, which means that the subsurface crack propagates to all directions but not just along the direction of the load movement.

Acknowledgements

This work was supported by the National Natural Science Foundation of China under agreement 51675025. The authors would like to thank the reviewers' helpful and valuable comments for the accomplishment of this paper.

References

[1] A. Heng, S. Zhang, A.C.C. Tan, J. Mathew, Rotating machinery prognostics: State of the art, challenges and opportunities, Mech Syst Signal Pr, 23 (2009) 724-739.

[2] J. Lee, F.J. Wu, W.Y. Zhao, M. Ghaffari, L.X. Liao, D. Siegel, Prognostics and health management design for rotary machinery systems-Reviews, methodology and applications, Mech Syst Signal Pr, 42 (2014) 314-334.

[3] Y. Ding, N.F. Rieger, Spalling formation mechanism for gears, Wear, 254 (2003) 1307-1317.

[4] Y. Ding, J.A. Gear, Spalling depth prediction model, Wear, 267 (2009) 1181-1190.

[5] J.W. Blake, H.S. Cheng, A Surface Pitting Life Model for Spur Gears: Part I—Life Prediction,

Journal of Tribology, 113 (1991) 712-718.
[6] N.E. Dowling, Mechanical behavior of materials : engineering methods for deformation, fracture, and fatigue Prentice Hall Englewood Cliffs, N.J, 1993
[7] L.M. Keer, M.D. Bryant, A Pitting Model for Rolling Contact Fatigue, Journal of Lubrication Technology, 105 (1983) 198-205.
[8] Y. Ding, R. Jones, B. Kuhnell, Numerical analysis of subsurface crack failure beneath the pitch line of a gear tooth during engagement, Wear, 185 (1995) 141-149.
[9] K. Komvopoulos, S.S. Cho, Finite element analysis of subsurface crack propagation in a half-space due to a moving asperity contact, Wear, 209 (1997) 57-68.
[10] K. Aslantas, S. Tasgetiren, A study of spur gear pitting formation and life prediction, Wear, 257 (2004) 1167-1175.
[11] Y.-J. Yang, L. Yang, H.-K. Wang, S.-P. Zhu, H.-Z. Huang, Finite Element Analysis for Turbine Blades with Contact Problems, Int J Turbo Jet Eng, 2015.
[12] Y. Hu, Y. Shao, Z. Chen, M.J. Zuo, Transient meshing performance of gears with different modification coefficients and helical angles using explicit dynamic FEA, Mech Syst Signal Pr, 25 (2011) 1786-1802.
[13] A. Ural, G. Heber, P.A. Wawrzynek, A.R. Ingraffea, D.G. Lewicki, J.B.C. Neto, Three-dimensional, parallel, finite element simulation of fatigue crack growth in a spiral bevel pinion gear, Engineering Fracture Mechanics, 72 (2005) 1148-1170.
[14] T. Lin, S. Zhong, L. Shen, Three-dimensional crack propagation simulation and life prediction in tooth root of cylindrical gear, Journal of Chongqing University (Natural Science Edition), 35 (2012) 1-7.
[15] G. Xu, F. Sadeghi, Spall initiation and propagation due to debris denting, Wear, 201 (1996) 106-116.
[16] A.F. Bower, K.L. Johnson, The influence of strain hardening on cumulative plastic deformation in rolling and sliding line contact, J Mech Phys Solids, 37 (1989) 471-493.
[17] K.L. Johnson, The Mechanics of Plastic Deformation of Surface and Subsurface Layers in Rolling And Sliding Contact, Key Engineering Materials, 33 (1989) 17-34.
[18] W. Cheng, H.S. Cheng, T. Mura, L.M. Keer, Micromechanics Modeling of Crack Initiation Under Contact Fatigue, Journal of Tribology, 116 (1994) 2-8.
[19] Y.S. Kang, F. Sadeghi, M.R. Hoeprich, A finite element model for spherical debris denting in heavily loaded contacts, J Tribol-t Asme, 126 (2004) 71-80.
[20] N.K. Arakere, N. Branch, G. Levesque, V. Svendsen, N.H. Forster, Rolling Contact Fatigue Life and Spall Propagation of AISI M50, M50NiL, and AISI 52100, Part II: Stress Modeling, Tribology Transactions, 53 (2009) 42-51.
[21] J. Lemaitre, A Course On Damage Mechanics, Springer-Verlag, New York, 1992.
[22] W. Prager, The theory of plasticity: a survey of recent achievements, Proceedings of the Institution of Mechanical Engineers, 169 (1955) 41-57.